

RESEARCH ARTICLE | JUNE 05 2023

## Room-temperature synthesis of 2D-Ti<sub>3</sub>C<sub>2</sub>T<sub>x</sub> nano-sheets by organic base treatment

Sunaina Rafiq ; Alessandra Gentili; Maria Assunta Navarra; ... et. al



*J. Chem. Phys.* 158, 214706 (2023)

<https://doi.org/10.1063/5.0146821>




View  
Online




Export  
Citation

CrossMark



**The Journal of Chemical Physics**  
Special Topic: Adhesion and Friction

**Submit Today!**



# Room-temperature synthesis of 2D-Ti<sub>3</sub>C<sub>2</sub>T<sub>x</sub> nano-sheets by organic base treatment

Cite as: J. Chem. Phys. 158, 214706 (2023); doi: 10.1063/5.0146821

Submitted: 24 February 2023 • Accepted: 12 May 2023 •

Published Online: 5 June 2023



View Online



Export Citation



CrossMark

Sunaina Rafiq,<sup>1,a)</sup> Alessandra Gentili,<sup>2</sup> Maria Assunta Navarra,<sup>2</sup> Corrado Zamparelli,<sup>2</sup>   
Maria Grazia Betti,<sup>1</sup> Riccardo Frisenda,<sup>1,a)</sup> and Carlo Mariani<sup>1</sup>

## AFFILIATIONS

<sup>1</sup>Dipartimento di Fisica, Sapienza Università di Roma, P. le Aldo Moro 2, 00185 Rome, Italy

<sup>2</sup>Dipartimento di Chimica, Hydro-Eco Research Center, Sapienza Università di Roma, P. le Aldo Moro 2, 00185 Rome, Italy

**Note:** This paper is part of the JCP Special Topic on Chemical Physics of Electrochemical Energy Materials.

**a) Authors to whom correspondence should be addressed:** [sunaina.rafiq@uniroma1.it](mailto:sunaina.rafiq@uniroma1.it) and [Riccardo.frisenda@uniroma1.it](mailto:Riccardo.frisenda@uniroma1.it)

## ABSTRACT

The growing demand for improved electrochemical performance in energy storage systems has stimulated research into advanced two-dimensional (2D) materials for electrodes. In this work, we obtain a layered MXene compound by exfoliating a titanium aluminum carbide precursor using tetramethylammonium hydroxide (TMAOH) ions in a full room temperature process followed by manual shaking. The hexagonal crystal structure and composition of the layered materials are characterized using different techniques. X-Ray diffraction shows the formation of 2D nano-sheets before and after the TMAOH treatment via its characteristic (002) diffraction peak, bringing to light an increase in the interlayer spacing after treatment. Scanning electron microscopy images confirm the layered morphology, whose composition is determined by energy dispersive x-ray analysis for the bulk material and by x-ray photoelectron spectroscopy for the surface of the obtained compounds. This study demonstrates a promising route to enhance delamination of this MXene 2D material in a low-cost room-temperature approach.

Published under an exclusive license by AIP Publishing. <https://doi.org/10.1063/5.0146821>

## I. INTRODUCTION

Two-dimensional (2D) materials have attracted great interest in the past few years due to their unique properties in comparison with their bulk form. Many novel 2D materials have emerged, including graphene,<sup>1</sup> transition metal dichalcogenides (TMDs),<sup>2</sup> and transition metal oxides (TMOs).<sup>3</sup> MXenes have recently emerged as a hot topic and grown rapidly as a novel 2D material family, currently containing about 30 members with various chemical compositions and orders, since it was discovered in 2011 by Naguib *et al.*<sup>4</sup> A large group of 2D transition metal carbides, nitrides, and carbonitrides classified as MXenes can be synthesized by treating the MAX phases with a wet hydrofluoric chemical. The general formula of MXene is M<sub>n+1</sub>X<sub>n</sub>T<sub>x</sub>, derived from the M<sub>n+1</sub>AX<sub>n</sub> phase, where “M” corresponds to an early transition metal, such as V and Ti, “A” is from elements such as Si and Al, “X” is nitrogen and/or carbon, and “n” is an integer (n = 1, 2, 3). T<sub>x</sub> stands for surface terminations (=O, OH, and F) that often occur as a result of the wet chemical etching techniques used to fabricate MXenes

from their MAX phase precursors.<sup>5,6</sup> These MAX phases are formed by stacked hexagonal planes (space group P63/mmc). However, the bond among M–X atoms is much stronger than the bond among M–A atoms, which makes it possible to remove the A element using specific chemical etchants in the MAX compound.<sup>7</sup> The Ti<sub>3</sub>C<sub>2</sub>T<sub>x</sub> phase is the most studied among MXenes known for its 2D nature, metallic conductivity, and hydrophilicity, and it can be obtained by extracting aluminum from the MAX Ti<sub>3</sub>AlC<sub>2</sub> phase.<sup>8</sup> The flake size, structure, and electronic properties of MXenes can depend on the different etchants used for exfoliation (NaF + HCl, HF, LiF + HCl, etc.) and on the intercalation conditions.<sup>9–11</sup> Halim *et al.* proposed to use ammonium bifluoride (NH<sub>4</sub>HF<sub>2</sub>) as an etchant to exfoliate the MAX phase.<sup>12</sup> Ghidui *et al.* reported the etching of Al from Ti<sub>3</sub>AlC<sub>2</sub> using LiF salts and HCl, providing a procedure for MXene synthesis.<sup>13</sup> MXenes have unique properties due to their variable chemistry and structural diversity,<sup>14,15</sup> which has led to their use in a wide range of potential applications,<sup>16</sup> including Li-ion batteries (LIBs),<sup>17–19</sup> supercapacitors,<sup>13,19,20</sup> and photocatalysis.<sup>21</sup> Ti<sub>3</sub>C<sub>2</sub>T<sub>x</sub> is hence considered promising for energy storage applications, mainly

as electrode materials for supercapacitors and also as negative electrode material for lithium-ion batteries.<sup>4,22,23</sup> Although electrodes produced by multilayer-MXene with narrow interplanar distance exhibit slow kinetics and low capacity, restacking of MXene flakes further reduces capacity. Furthermore,  $-F$  ion could be hazardous to the charge storage process.<sup>24</sup> Delaminated  $Ti_3C_2T_x$  shows better electrochemical performances and helps in reduction of the energy barrier for usage in different energy storage applications.<sup>25-27</sup>

Different strategies on surface modification and interlayer spacing modulation have been employed to improve the electrochemical performance of MXenes.<sup>28</sup> In this study, we demonstrate new synthesis routes to exfoliate multilayers MXene by selective etching with aqueous fluoride acid and delamination with tetramethylammonium hydroxide (TMAOH) treatment at room-temperature while doing manual shaking. During the synthesis, the chemically etched MXene forms an accessible interlayer space, which provides plenty

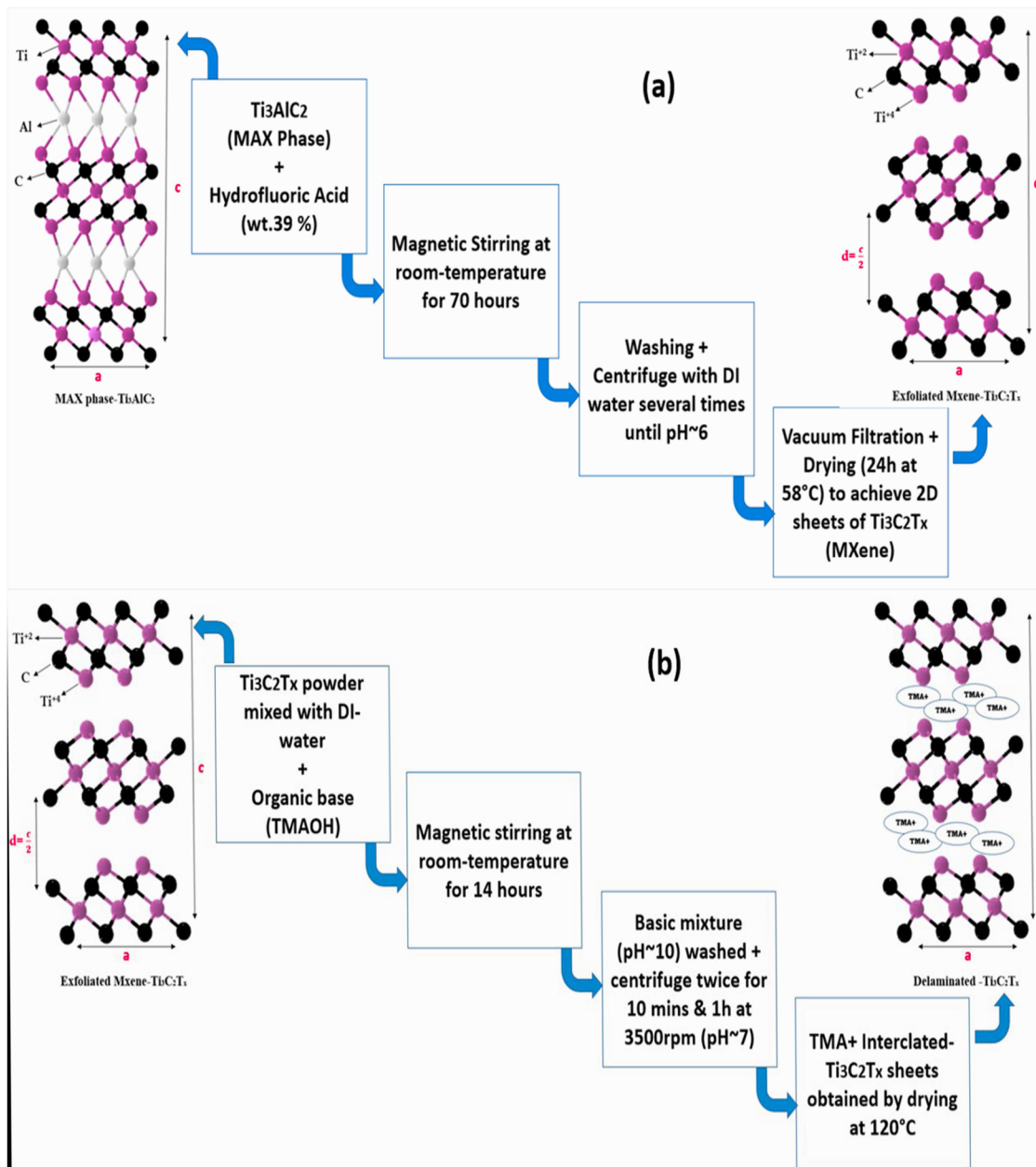


FIG. 1. Flowchart of the synthesis process of (a)  $Ti_3C_2T_x$  MXene and (b) delaminated- $Ti_3C_2T_x$  MXene.

of active sites for ion storage and can have a strong impact on the expected electrochemical performance. We intercalate  $\text{TMA}^+$  ions into originally made  $\text{Ti}_3\text{C}_2\text{T}_x$  that interacts with the functional groups, weakens the bonds between the layers, and enlarges the interlayer spacing to further improve the quality of MXene as the material for potential energy storage applications.

## II. EXPERIMENTAL METHODS

For the preparation of 2D MXene sheets, 3 g of  $\text{Ti}_3\text{AlC}_2$  powder (>98 wt. % purity) was treated in HF-solution (49 wt. %, 70 ml) into Teflon bottle and continuously stirred on a magnetic plate for 70 h at room temperature. After completion, the product was repeatedly rinsed with de-ionized (DI) water, and then, slurry was separated by repeatedly centrifuging it at 7000 rpm for 7 min to remove the remaining acidic residues until the pH  $\sim 6$  was achieved. The completely washed slurry was then dried in a vacuum oven for 24 h at  $58^\circ\text{C}$ . The final product was etched  $\text{Ti}_3\text{C}_2\text{T}_x$  MXene sheets. An organic base, Tetramethylammonium hydroxide (TMAOH), was used to delaminate the  $\text{Ti}_3\text{C}_2\text{T}_x$  nano-sheets. 100 g of multi-layered  $\text{Ti}_3\text{C}_2\text{T}_x$  MXene powder was mixed into 10 ml of de-ionized (DI) water separately, containing 0.46 ml Tetramethylammonium Hydroxide (TMAOH) in a 20 ml glass vial. Then, the vial was placed on a stirrer plate and was stirred 14 h at RT. After 14 h, the basic mixture was moved to centrifuging tubes and centrifuged twice for 10 min to lower the pH from  $\sim 10$  to  $\sim 7$ . The stable colloidal solution of MXene was achieved by doing further centrifuge of solution for 1 h.  $\text{Ti}_3\text{C}_2\text{T}_x$  MXene nanosheets were delaminated after shaking it manually, and then, the collected sediment was dried in oven at  $120^\circ\text{C}$ . The fabrication process of exfoliated and delaminated  $\text{Ti}_3\text{C}_2\text{T}_x$  MXene is schematically shown in Fig. 1. The conversion of pristine  $\text{Ti}_3\text{AlC}_2$  into  $\text{Ti}_3\text{C}_2\text{T}_x$  MXene that exhibits a loose multi-layered structure indicates the successful extraction of Al layers from  $\text{Ti}_3\text{AlC}_2$ , confirming the treatment was successful. Furthermore, delaminating the multilayer- $\text{Ti}_3\text{C}_2\text{T}_x$  by using the TMAOH solvent is to expand the inter-layer spacing and weaken the bonds/interaction by causing swelling through the chemical intercalation of large tetramethylammonium ions ( $\text{TMA}^+$ ) between the  $\text{Ti}_3\text{C}_2\text{T}_x$ -layers. Meanwhile, the large, intercalated  $\text{TMA}^+$  ions also reduced the F-content between the layers and terminated with  $-\text{O}$  and  $-\text{OH}$  groups.

### A. Characterization techniques

Structural diffraction measurements were made in a X-Ray Diffraction (XRD) diffractometer using monochromatic  $\text{Cu-K}\alpha$  radiation at a wavelength ( $\lambda = 1.5405$  nm), under 200 mA current and 40 kV voltage source, with  $2\theta$  ranging from  $5^\circ$  to  $65^\circ$ . Scanning electron microscopy (SEM) was used to investigate the particle size and morphology of the samples, while the chemical composition of the samples was studied using Energy Dispersive X-ray spectroscopy (EDX). The X-Ray Photoelectron Spectroscopy (XPS) experiments took place in an UHV chamber with a base pressure in the low  $10^{-10}$  mbar range. X-ray photon source (PSP TA10)  $\text{MgK}\alpha$  with  $h\nu = 1253.6$  eV was used. A hemispherical VG Microtech Clam-2 electron analyzer with an overall energy resolution  $\leq 1$  eV and constant pass energy mode set at 50 eV was used to measure the photoelectrons. The  $\text{Au}4f_{7/2}$  core-level was set to 84.0 eV BE to calibrate

the binding energy scale on a freshly sputtered gold foil in electrical contact with the sample.

## III. RESULTS AND DISCUSSION

The crystallographic structure of the samples in the different treatment phases is studied by XRD in the  $2\theta$  range from  $5^\circ$  to  $65^\circ$ , as shown in Fig. 2. The pristine  $\text{Ti}_3\text{AlC}_2$  crystal phase is a typical hexag-

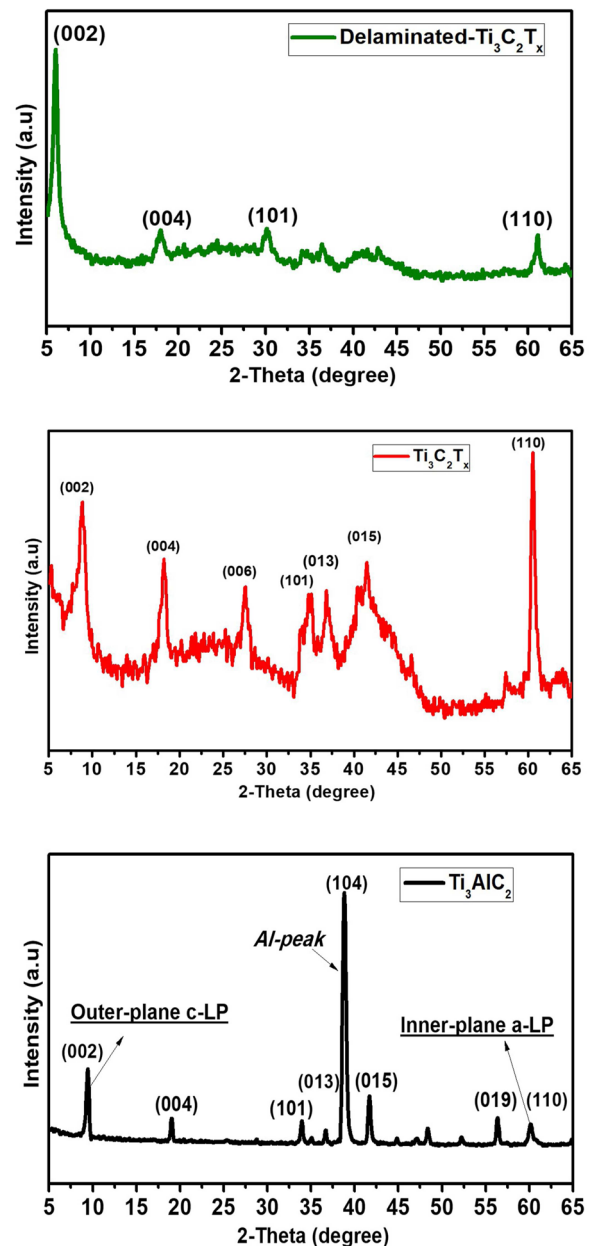


FIG. 2. XRD pattern of (a) bulk MAX ( $\text{Ti}_3\text{AlC}_2$ ) phase (bottom panel). (b) Exfoliated (middle panel) and (c) delaminated (top panel) MXene ( $\text{Ti}_3\text{C}_2\text{T}_x$ ).

**TABLE I.** Lattice parameters (LP), *c/a* ratio, average crystallite sizes, and interplanar spacing estimate from the XRD pattern.

Sample	<i>a</i> (Å)	<i>c</i> (Å)	<i>c/a</i>	Average crystallite size (nm)	Interlayer (d-spacing) by (hk0) and (00l) planes
Ti <sub>3</sub> AlC <sub>2</sub>	3.09	18.8	6.08	54	1.54 (a-LP) 9.4 (c-LP)
Ti <sub>3</sub> C <sub>2</sub> T <sub>x</sub>	3.04	20	6.57	13	1.52 (a-LP) 10 (c-LP)
Delaminated-Ti <sub>3</sub> C <sub>2</sub> T <sub>x</sub>	3.02	29.4	9.73	18	1.51 (a-LP) 14.7 (c-LP)

onal (P63/mmc) crystal structure (Fig. 2, bottom panel).<sup>29</sup> After HF etching, a broadening and intensity reduction of the diffraction peaks is observed for Ti<sub>3</sub>C<sub>2</sub>T<sub>x</sub> (Fig. 2, middle panel), indicating a slightly lower crystallinity. The peak at 38.7° corresponding to the (104) plane of Ti<sub>3</sub>AlC<sub>2</sub> almost disappears, indicating that “Al” has been extracted from the Ti<sub>3</sub>AlC<sub>2</sub> structure, which is strong evidence that the MAX phase is etched and converted into MXene nano-sheets. The (00l)-family peaks (002, 004, and 006) present different intensities with respect to the MAX phase, confirming its different layered structure. In particular, they are shifted to lower angles compared to their position before treatment, which results in larger interlayer-spacing (d-spacing) between the Ti<sub>3</sub>C<sub>2</sub>T<sub>x</sub> layers, according to the Bragg law, as reported in Table I. The *a* and *c* lattice parameters are representing the inner and outer planes of the Ti<sub>3</sub>C<sub>2</sub>T<sub>x</sub> structure. The *c*-lattice parameter shifts from 18.8 to 20 Å due to extraction of Al layers from the starting material

**TABLE II.** The variations at different planes of all the samples.

Samples	Position 2θ			Crystallite size (nm)
	(deg)	(hkl)	β (rad)	
Ti <sub>3</sub> AlC <sub>2</sub>	9.4	(002)	0.098	80.97
	19.0	(004)	0.12	68.17
	33.9	(101)	0.16	52.75
	36.6	(013)	0.16	53.13
	38.7	(104)	0.12	71.24
	41.6	(015)	0.19	43.16
	48.3	(017)	0.20	44.23
	56.3	(019)	0.20	45.78
	60.1	(110)	0.39	23.32
	8.8	(002)	0.63	12.57
Ti <sub>3</sub> C <sub>2</sub> T <sub>x</sub>	18.3	(004)	0.47	16.59
	27.5	(006)	0.63	12.24
	35.0	(101)	0.63	12.02
	36.9	(013)	0.63	11.95
	60.5	(110)	0.48	14.28
Delaminated-Ti <sub>3</sub> C <sub>2</sub> T <sub>x</sub>	6.0	(002)	0.49	16.18
	18.0	(004)	0.53	14.77
	30.1	(101)	0.35	21.90
	61.1	(110)	0.39	17.52

after HF-assisted exfoliation, causing an increase in layer spacing. The new sharp and broad diffraction peak at 2θ ~ 27.5° of the (006) plane shows the characteristic TiO<sub>2</sub> rutile phase in which =O attached with Ti<sup>4+</sup> on the surface in oxides form.<sup>30</sup> In addition, the diffraction peaks at 36.9° is due to the presence of the Al<sub>2</sub>O<sub>3</sub> nanocrystal on the surface of MXene, which form because of the residual Al<sup>3+</sup> that follows the migration of inside water to the surface and separate out during the oven-drying process.<sup>31</sup> In the crystal structure, the peaks at 2θ ~ 35°, 36.9°, and 60.5°, which correspond to the (101), (013), and (110) planes, show the characteristics of titanium carbide.<sup>32</sup> These peaks are already present in the starting material with relatively low intensity, but after etching, we note that the intensity increases and they shift to higher angles. This shift might be caused by two possible effects: strong electrostatic interaction and ion-exchange mechanism in the crystal structure of Ti<sub>3</sub>C<sub>2</sub>T<sub>x</sub>.

After TMAOH treatment (Fig. 2, top panel), high-index diffraction peaks drastically weaken, confirming that multi-layer Ti<sub>3</sub>C<sub>2</sub>T<sub>x</sub> MXene have been exfoliated, further evidence for the conversion to MXene with swollen layers and inter-layer modification. The (002) peak shifts to lower angles from 2θ ~ 8.8° to 2θ ~ 6° with respect to the MAX phase, indicating the further increase of d-spacing (*d* = 14.7 Å), and the *c*-lattice parameter between nanosheets increases from 20 to 29.4 Å. This further increase in interlayer spacing is a clear indication that the TMA<sup>+</sup> ions intercalate and induce significant spontaneous swelling, which, in turn, weakens the bonds between MXene layers.

The changes occurring in the inner and outer planes of the structure, and all the parameters we calculated due to this structural change are summarized in Tables I and II. The lattice parameters of all the samples are calculated by the equation of plane spacing for the hexagonal crystal structure,<sup>33</sup>

$$\frac{1}{d^2} = \frac{4}{3} \left( \frac{h^2 + hk + k^2}{a^2} \right) + \frac{l^2}{c^2},$$

where “*hkl*” are the Miller indices of a given plane. The particle size is calculated from the broadening of the diffraction peak by using the Scherrer’s formula,  $D = \frac{k\lambda}{\beta \cos \theta}$ , while the interlayer spacing or interplanar distance between the layers of the crystal structure are calculated by the Bragg’s law,  $d = \frac{n\lambda}{2 \sin \theta}$ .<sup>34</sup>

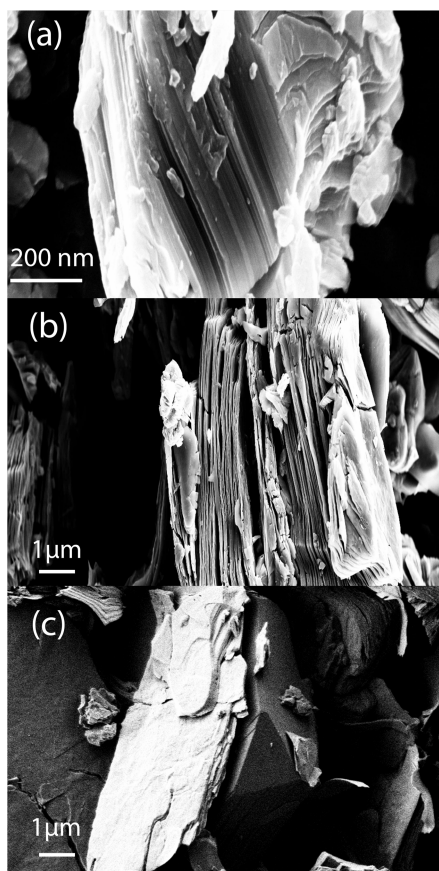


**FIG. 3.** SEM images of (a)  $\text{Ti}_3\text{AlC}_2$  powder, (b) multi-layered  $\text{Ti}_3\text{C}_2\text{T}_x$  powder synthesized with 49 wt. % HF, and (c)  $\text{Ti}_3\text{C}_2\text{T}_x$  powder obtained using TMAOH treatment.

The compounds in the different treatment phases are imaged by SEM, showing their general morphology.  $\text{Ti}_3\text{AlC}_2$  before etching shows a compact layered structure in the form of bulk material [Fig. 3(a)]; the layered structure of  $\text{Ti}_3\text{C}_2\text{T}_x$  after HF-treatment is maintained [Fig. 3(b)] as also after manual shaking in TMAOH [Fig. 3(c)].

The EDX analysis carried out on all the compounds allows the estimate of the different compositional concentrations (%) as reported in Table III. Chemical analysis by EDX reveals that most of Al was eliminated, although some F and O elements are still present in the  $\text{Ti}_3\text{C}_2\text{T}_x$  sample, which is consistent with the following XPS results. The results from EDX show that Al layers are replaced by  $-\text{O}$  and/or  $-\text{F}^{35}$  that is confirmed by the increase in percentage after etching. Furthermore, the  $-\text{F}$  concentration decreases after TMAOH treatment.

XPS measurements are used to investigate the surface and chemical states of the elements of the  $\text{Ti}_3\text{C}_2\text{T}_x$  nanosheets. The survey spectra for all the samples are shown in Fig. 4(a): we observe the presence of the expected elements (Ti2p, C1s, O1s, F1s, and Al2p), although part of the C signal may derive from residual contamination on the surfaces. The O1s signal may derive from residual contamination, from surface-terminations on  $\text{Ti}_3\text{C}_2\text{T}_x$  surface, and from the oxidation of the  $\text{Ti}_3\text{C}_2\text{T}_x$  MXene. Fluorine derives from the surface-termination of  $\text{Ti}_3\text{C}_2\text{T}_x$  MXene and partly from the residual reactants.<sup>36</sup>

In the survey scans, the Al2p core level is visible in the MAX phase, but it is quenched after etching, evidence of proper removal of Al. The at. % ratio of all the elements present on the surface is estimated from the XPS survey spectra by fitting each core level with a pseudo-Voigt line shape (Gaussian-Lorentzian curve, associated with the experimental uncertainty and intrinsic excitation lifetime, respectively) after removal of a Shirley background, whose results are presented in Table III. We note that the percentages we calculated of all the elements on the surface have changed after etching and TMAOH treatment, although they are not fully in line with the expected chemical composition of  $\text{Ti}_3\text{AlC}_2$ . This discrepancy with the concentration of elements as derived from EDX (also presented in Table III) points at a slightly different surface composition as measured by XPS (very surface sensitive) with respect to the bulk of the materials.

The high-resolution XPS Ti2p spectra for all samples together with their peak fits are shown in Fig. 5. We know that a variety of surface-terminations exists on the surface of materials after exfoliation and delamination. This can be reflected in chemical shifted components of the Ti2p core levels due to different surface-groups attached to the samples, marked by Roman numerals in Fig. 4(b), where the Ti atoms are colored in blue, oxygen in red, hydrogen in white, and fluorine in blue. We summarize it as moieties, defined as follows: (1) Moiety I corresponds to Ti atoms attached to C atoms

**TABLE III.** The percentage of elements present in all the samples after the formation of MXene ( $\text{Ti}_3\text{C}_2\text{T}_x$ ).

Samples	Analysis	Chemical elements (concentration %)				
		Ti%	C%	Al%	F%	O%
$\text{Ti}_3\text{AlC}_2$	EDX	45	36	13	...	6
	XPS	31	29	14	...	26
$\text{Ti}_3\text{C}_2\text{T}_x$	EDX	27	24	2	30	17
	XPS	40	35	...	15	12
Delaminated- $\text{Ti}_3\text{C}_2\text{T}_x$	EDX	35	21	...	9	33
	XPS	13	48	...	5	33

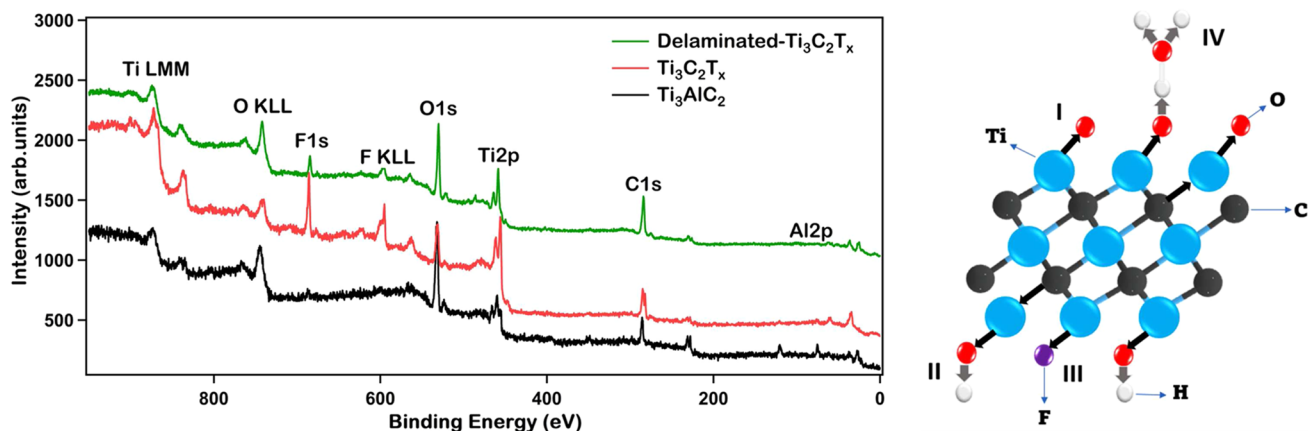


FIG. 4. (a) Survey spectra of the MAX phase (bottom), exfoliated (middle) and delaminated (top) MXene ( $Ti_3C_2T_x$ ); spectra are vertically stacked for clarity. (b) Top View schematic of a  $Ti_3C_2T_x$  structure showing various termination sites of  $-T_x$  and Moieties.

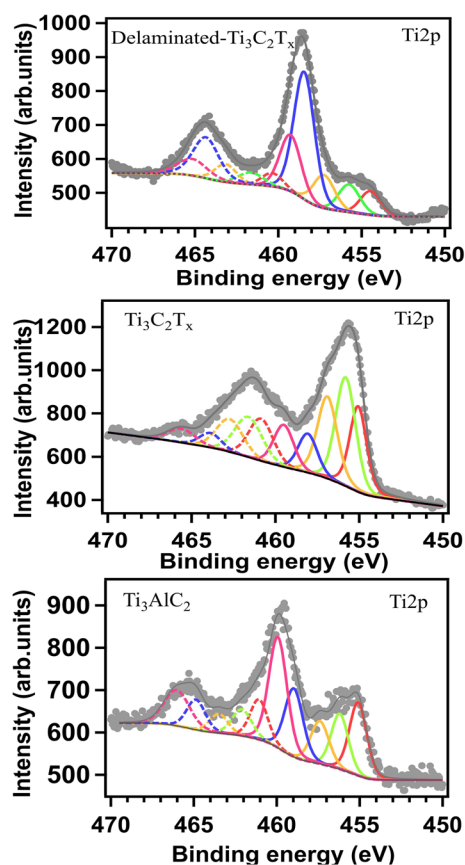


FIG. 5. High-resolution  $Ti2p$  spectra of all the samples.

and one bridging oxygen atom, e.g.,  $Ti_3C_2O_x$ . (2) Moiety II refers to Ti attached with C atoms and an  $-OH$  group, e.g.,  $Ti_3C_2(OH)_x$ . (3) Moiety III refers to Ti attached with C and F atoms, e.g.,  $Ti_3C_2F_x$ . (4) Moiety IV refers to Ti atoms bonded to OH-terminations, which, in turn, are comparatively strong physisorbed to water molecules that form  $OH-H_2O$  complexes (called  $H_2O_{ads}$ ).<sup>37</sup>

The  $Ti\ 2p$  XPS peaks Fig. 5 for all the samples are deconvoluted into Gaussian-Lorentzian fitting doublets, with the expected spin-orbit splitting and intensity ratio.<sup>38</sup> The  $Ti2p$  components exhibit different oxidation states of titanium on the surface of the MAX and MXene phases, in general agreement with the oxidation species observed in the literature.<sup>38–40</sup> They are associated with  $TiC$ ,  $Ti^{+2}$ ,  $Ti^{+3}$ ,  $Ti^{+4}$ , and  $Ti^{+4-x}$  at different binding energies due to the different valence state of Ti in the compounds, in agreement with our experimental data, whose fitting results are reported in Table IV.

We note that the BE of  $Ti2p$  peaks in the  $Ti_3C_2T_x$  sample after etching slightly decreases, possibly due to introducing defects between the layers and/or replacement of Al layers by more electro-negative surface terminations, such as  $-O$ ,  $-OH$ , and  $-F$ .<sup>29</sup> Room-temperature TMAOH treatment of delaminated- $Ti_3C_2T_x$  colloidal solution undergoes spontaneous reaction with oxygen and/or water. This suggests that even if care is taken to restrict its exposure to air, oxidized titanium species, including  $TiO_2$  and also a small amount of  $TiO_{2-x}F_{2x}$  bond in the form of oxyfluoride species, may be located on the surface of the produced  $Ti_3C_2T_x$  powder. In delaminated- $Ti_3C_2T_x$  MXene, all the  $Ti2p$  peaks are shifted to higher BE except  $Ti-C$  (see Table IV). The increased BE is probably due to the incorporated  $TMA^+$  ions between the layers, while the reduced BE of  $Ti-C$  could be associated with a bond weakening after swelling. Further notable point after TMAOH treatment is the clearly visible  $-F$  component decrease in delaminated- $Ti_3C_2T_x$  spectra, suggesting that F is replaced by O significantly, in agreement with the EDX results.

**TABLE IV.** Parameters obtained for the Ti2p Gaussian–Lorentzian curve fitting of all the samples.

Samples	Region	B.E 2p3/2	B.E 2p1/2	FWHM (eV)	Component atomic %	
Ti <sub>3</sub> AlC <sub>2</sub>	Ti2p	455.1	461.1	1.3	1.4	21%
		456.2	462.1	1.2	1.4	15%
		457.4	463.5	1.3	1.4	12%
		459.0	464.9	1.3	1.4	19%
		459.9	466.0	1.3	1.8	33%
Ti <sub>3</sub> C <sub>2</sub> T <sub>x</sub>	Ti2p	455.2	461.1	1.3	1.7	34%
		456.1	462.0	1.3	1.8	21%
		456.9	462.9	1.5	1.8	22
		458.2	464.1	1.5	1.7	10%
		459.7	465.8	1.5	2.0	13%
Delaminated-Ti <sub>3</sub> C <sub>2</sub> T <sub>x</sub>	Ti2p	454.5	460.4	1.4	1.5	9%
		455.8	461.7	1.5	1.8	10%
		457.3	463.2	1.4	1.5	14%
		458.5	464.4	1.4	1.8	46%
		459.3	465.2	1.5	2.1	21%

#### IV. CONCLUSIONS

We successfully synthesized 2D multilayered Ti<sub>3</sub>C<sub>2</sub>T<sub>x</sub> MXene nanosheets by intercalating TMA<sup>+</sup> ions into MXene at room-temperature and by doing manual shaking, instead of using ultrasonication methods. The TMAOH organic solvent weakens the bonds between the layers, and the intercalated TMA<sup>+</sup> ions interact with the functional group and determine the larger interlayer distance between the layers. The XRD estimated c-lattice parameter increases from 18.8 to 20 Å after etching of the Al-layer and further to 29.4 Å after TMAOH treatment. The TMAOH treatment removes Al and reduces the F-content from the surface of the nanosheets, as revealed by EDX spectroscopy. Reduction of F is an important result, as fluorine high electronegativity would act as a passivating layer for any potential use as electrode material. X-ray photoemission, while showing elemental composition in agreement with EDX, enlightens a slightly different surface composition with respect to the bulk. High-resolution Ti2p core-level spectra recorded for the compounds allow us to understand the nature of chemical bonding in all samples. This work is propaedeutic for the development of advanced and improved 2D materials as promising candidates for electronics and energy storage applications.

#### ACKNOWLEDGMENTS

This work was partially supported by the PRIN FERMAT (Grant No. 2017KFY7XF) from Italian Ministry MUR and by Sapienza Ateneo funds.

#### AUTHOR DECLARATIONS

##### Conflict of Interest

The authors have no conflicts to disclose.

#### Author Contributions

**Sunaina Rafiq:** Conceptualization (equal); Formal analysis (equal); Investigation (lead); Methodology (lead); Software (equal); Writing – original draft (lead). **Alessandra Gentili:** Formal analysis (equal); Methodology (equal); Resources (equal); Writing – review & editing (equal). **Maria Assunta Navarra:** Formal analysis (equal); Investigation (equal); Resources (equal); Writing – review & editing (equal). **Corrado Zamparelli:** Formal analysis (equal); Software (equal). **Maria Grazia Betti:** Resources (equal); Supervision (equal); Writing – review & editing (equal). **Riccardo Frisenda:** Formal analysis (equal); Software (equal); Supervision (equal); Writing – review & editing (equal). **Carlo Mariani:** Funding acquisition (equal); Project administration (equal); Resources (equal); Supervision (equal); Writing – review & editing (equal).

#### DATA AVAILABILITY

The data that support the findings of this study are available from the corresponding authors upon reasonable request.

#### REFERENCES

- M. Peplow, *Nature* **503**(7476), 327 (2013).
- M. Chhowalla, Z. Liu, and H. Zhang, *Chem. Soc. Rev.* **44**(9), 2584 (2015).
- C. J. Zhang, S. J. Kim, M. Ghidui, M.-Q. Zhao, M. W. Barsoum, V. Nicolosi, and Y. Gogotsi, *Adv. Funct. Mater.* **26**(23), 4143 (2016).
- M. Naguib, M. Kurtoglu, V. Presser, J. Lu, J. Niu, M. Heon, L. Hultman, Y. Gogotsi, and M. W. Barsoum, *Adv. Mater.* **23**(37), 4248 (2011).
- M. A. Iqbal, A. Tariq, A. Zaheer, S. Gul, S. I. Ali, M. Z. Iqbal, D. Akinwande, and S. Rizwan, *ACS Omega* **4**(24), 20530 (2019).
- L. Verger, V. Natu, M. Carey, and M. W. Barsoum, *Trends Chem.* **1**(7), 656 (2019).
- M. Magnuson and M. Mattesini, *Thin Solid Films* **621**, 108 (2017).
- S. Rafiq, H. Ahmad, M. Rani, and R. Syed, “Structural and morphological analysis for cerium (Ce<sup>+3</sup>) doped intercalated 2D MXene,” *SPIE* **2020**, 1156103



- <sup>9</sup>A. Lipatov, M. Alhabeb, M. R. Lukatskaya, A. Bosen, Y. Gogotsi, and A. Sinitskii, *Adv. Electron. Mater.* **2**(12), 1600255 (2016).
- <sup>10</sup>A. Feng, Y. Yu, Y. Wang, F. Jiang, Y. Yu, L. Mi, and L. Song, *Mater. Des.* **114**, 161 (2017).
- <sup>11</sup>F. Liu, A. Zhou, J. Chen, J. Jia, W. Zhou, L. Wang, and Q. Hu, *Appl. Surf. Sci.* **416**, 781 (2017).
- <sup>12</sup>J. Halim, M. R. Lukatskaya, K. M. Cook, J. Lu, C. R. Smith, L.-Å. Näslund, S. J. May, L. Hultman, Y. Gogotsi, and P. Eklund, *Chem. Mater.* **26**(7), 2374 (2014).
- <sup>13</sup>M. Ghidui, M. R. Lukatskaya, M.-Q. Zhao, Y. Gogotsi, and M. W. Barsoum, *Nature* **516**(7529), 78 (2014).
- <sup>14</sup>M. Berdych, C. E. Shuck, D. Pinto, A. Mohamed, E. Precetti, D. Grayson, B. Anasori, N. Kurra, and Y. Gogotsi, *Chem. Mater.* **31**(9), 3324 (2019).
- <sup>15</sup>H. Tang, Y. Yang, R. Wang, and J. Sun, *J. Mater. Chem. C* **8**(18), 6214 (2020).
- <sup>16</sup>J.-C. Lei, X. Zhang, and Z. Zhou, *Front. Phys.* **10**, 276 (2015).
- <sup>17</sup>J. Luo, X. Tao, J. Zhang, Y. Xia, H. Huang, L. Zhang, Y. Gan, C. Liang, and W. Zhang, *ACS Nano* **10**(2), 2491 (2016).
- <sup>18</sup>D. Sun, M. Wang, Z. Li, G. Fan, L.-Z. Fan, and A. Zhou, *Electrochem. Commun.* **47**, 80 (2014).
- <sup>19</sup>X. Li, Z. Huang, C. E. Shuck, G. Liang, Y. Gogotsi, and C. Zhi, *Nat. Rev. Chem.* **6**(6), 389 (2022).
- <sup>20</sup>M. Zhu, Y. Huang, Q. Deng, J. Zhou, Z. Pei, Q. Xue, Y. Huang, Z. Wang, H. Li, and Q. Huang, *Adv. Energy Mater.* **6**(21), 1600969 (2016).
- <sup>21</sup>M. A. Iqbal, S. I. Ali, F. Amin, A. Tariq, M. Z. Iqbal, and S. Rizwan, *ACS Omega* **4**(5), 8661 (2019).
- <sup>22</sup>X. Li, Q. Li, Y. Hou, Q. Yang, Z. Chen, Z. Huang, G. Liang, Y. Zhao, L. Ma, and M. Li, *ACS Nano* **15**(9), 14631 (2021).
- <sup>23</sup>Y. Xie, M. Naguib, V. N. Mochalin, M. W. Barsoum, Y. Gogotsi, X. Yu, K.-W. Nam, X.-Q. Yang, A. I. Kolesnikov, and P. R. C. Kent, *J. Am. Chem. Soc.* **136**(17), 6385 (2014).
- <sup>24</sup>G. Li, L. Tan, Y. Zhang, B. Wu, and L. Li, *Langmuir* **33**(36), 9000 (2017).
- <sup>25</sup>V. Nicolosi, M. Chhowalla, M. G. Kanatzidis, M. S. Strano, and J. N. Coleman, *Science* **340**(6139), 1226419 (2013).
- <sup>26</sup>M. R. Lukatskaya, O. Mashtalir, C. E. Ren, Y. Dall'Agnese, P. Rozier, P. L. Taberna, M. Naguib, P. Simon, M. W. Barsoum, and Y. Gogotsi, *Science* **341**(6153), 1502 (2013).
- <sup>27</sup>O. Mashtalir, M. Naguib, V. N. Mochalin, Y. Dall'Agnese, M. Heon, M. W. Barsoum, and Y. Gogotsi, *Nat. Commun.* **4**(1), 1716 (2013).
- <sup>28</sup>X. Song, H. Wang, S. Jin, M. Lv, Y. Zhang, X. Kong, H. Xu, T. Ma, X. Luo, and H. Tan, *Nano Res.* **13**, 1659 (2020).
- <sup>29</sup>X. Wang and Y. Zhou, *J. Mater. Chem.* **12**(3), 455 (2002).
- <sup>30</sup>I. M. Joni, L. Nulhakim, and C. Panatarani, "Characteristics of TiO<sub>2</sub> particles prepared by simple solution method using TiCl<sub>3</sub> precursor," *J. Phys.: Conf. Ser.* (unpublished).
- <sup>31</sup>S. Rafiq, S. Awan, R.-K. Zheng, Z. Wen, M. Rani, D. Akinwande, and S. Rizwan, *J. Magn. Magn. Mater.* **497**, 165954 (2020).
- <sup>32</sup>P. Baviera, S. Harel, H. Gareem, and M. Grosbras, *Scr. Mater.* **44**(12), 2721 (2001).
- <sup>33</sup>B. D. Cullity, *Answers to Problems: Elements of X-Ray Diffraction* (Addison-Wesley Publishing Company, 1978).
- <sup>34</sup>W. Zaw, S. Oo, and H. H. Win, in *MERAL Portal*.
- <sup>35</sup>I. Habib, P. Ferrer, S. C. Ray, and K. I. Ozoemena, *J. Appl. Phys.* **126**(13), 134301 (2019).
- <sup>36</sup>Y. Lu, D. Li, and F. Liu, *Materials* **15**(1), 307 (2022).
- <sup>37</sup>J. Halim, K. M. Cook, M. Naguib, P. Eklund, Y. Gogotsi, J. Rosen, and M. W. Barsoum, *Appl. Surf. Sci.* **362**, 406 (2016).
- <sup>38</sup>V. Natu, M. Benchakar, C. Canaff, A. Habrioux, S. Célérier, and M. W. Barsoum, *Matter* **4**(4), 1224 (2021).
- <sup>39</sup>T. Koriukina, A. Kotronia, J. Halim, M. Hahlin, J. Rosen, K. Edström, and L. Nyholm, *ACS Omega* **7**(45), 41696 (2022).
- <sup>40</sup>B. Gou, L. Wang, B. Ye, C. Meng, X. Li, Q. Chen, T. Yang, and W. Xu, *J. Mater. Sci.: Mater. Electron.* **32**(10), 13081 (2021).